Journal of Power Sources 195 (2010) 2863–2869

Contents lists available at ScienceDirect

Journal of Power Sources

journal homepage: www.elsevier.com/locate/jpowsour

Ionic conducting behavior of solvent-free polymer electrolytes prepared from oxetane derivative with nitrile group

Yusuke Shintani, Hiromori Tsutsumi*

Department of Applied Chemistry, Faculty of Engineering, Yamaguchi University, 2-16-1 Tokiwadai, Ube 755-8611, Japan

ARTICLE INFO

Article history:
Received 19 September 2009
Received in revised form 7 November 2009
Accepted 10 November 2009
Available online 14 November 2009

Keywords:
Oxetane
Trimethylene oxide
Nitrile
Solid polymer electrolyte
Lithium ion

ABSTRACT

Polymer with trimethylene oxide (TMO) units prepared from ring-opening polymerization of an oxetane derivative is a candidate for the matrix of solid polymer electrolytes. We prepare an oxetane derivative with nitrile group, 3-(2-cyanoethoxymethyl)-3-ethyloxetane, CYAMEO. CYAMEO is polymerized by using a cationic initiator system. The structure of the resulted polymer, P(CYAMEO), is confirmed by NMR and FTIR spectroscopic techniques. Inorganic salts, such as lithium salts, can be dissolved in P(CYAMEO) matrix. FTIR and DSC results of P(CYAMEO)-based electrolyte films suggest that lithium ions in the P(CYAMEO) matrix interact with the nitrile side chains, mainly, and not with the oxygen atoms on the main chain of the P(CYAMEO). The conductivity at 30 °C for P(CYAMEO)-based electrolyte films, P(CYAME)10(LiX)1, is 19.6 μS cm^{-1} (X = $LiClO_4$), 6.59 μS cm^{-1} (BF_4), 6.54 μS cm^{-1} (CF_3SO_3), and 25.0 μS cm^{-1} ($N(CF_3SO_2)_2$). The rise in temperature from 30 °C to 70 °C increases their conductivity, about 30–40 times. The conductivity at 70 °C for P(CYAMEO)-based electrolyte films is 0.742 mS cm^{-1} (X = $LiClO_4$) and 0.703 mS cm^{-1} ($N(CF_3SO_2)_2$). Electrochemical deposition and dissolution of lithium on a nickel plate electrode are observed in the solvent-free three-electrode electrochemical cell with P(CYAMEO)10(LiX)1, (X = ClO_4 or $N(CF_3SO_2)_2$) electrolyte film at 55 °C.

1. Introduction

Polymer electrolytes are key materials for construction of lightweight, thin, and flexible batteries. Many types of polymer electrolytes have been investigated. Scrosati and Vincent categorized polymer electrolytes into five classes [1]. Polymer electrolytes categorized as "Class 1" consist of polymer as a matrix (quasi-solvent) and inorganic salt, such as lithium salt [1]. This simple system has some advantageous points for battery application, for example, no leakage of low-molecular weight compounds, *i.e.* plasticizer, from electrolyte films and lower flammability than normal organic electrolyte solutions. However, conductivity for polymer–inorganic salt systems is normally lower than for other polymer electrolyte system, such as gel electrolytes [2].

Many polymer compounds for "Class 1" polymer electrolytes have polyether structure, especially, polyethylene oxide (PEO) structure in their main chain and/or side chains. PEO and its derivatives are used as a polymer matrix for solid polymer electrolyte, because of their low glass transition temperature (T_g), the capability in forming solvation shells with cations, and commercial availability. However, the limitation of ion transport properties in PEO–lithium salt systems is a major obstacle for wide applications [3,4].

Some research groups have investigated new-type polyether-based electrolytes with trimethylene oxide (–$CH_2CH_2CH_2O$–, TMO) units [5–15]. Ye et al. prepared two monomers, 3-(2-cyanoethoxy)methyl- and 3-[(methoxytriethyleneoxy)]-methyl-3′-methyloxetane, and their polymers. The conductivity of their poly(oxetane)-based electrolyte at room temperature is about 10.7 μS cm^{-1}, while at 80 °C is 0.279 mS cm^{-1} [10–12]. They also prepared the hyperbranch poly(oxetane)-based electrolytes. The ionic conductivity measurements showed that the sample reaches a maximum ionic conductivity of 80 μS cm^{-1} at 30 °C and 0.74 mS cm^{-1} at 80 °C, respectively, after doping with $LiN(CF_3SO_2)_2$ [13]. Kerr et al. reported on a new comb branch polymer based on TMO side chains as a polymer electrolyte for potential application in lithium metal rechargeable batteries [14,15].

We have also investigated polymer electrolyte films with TMO structure and reported their conduction behavior [7–9]. In those investigations, we prepared the polymer with TMO structure by ring-opening polymerization of oxetane derivatives that is initiated with lithium salts. The highest conductivity for our systems is 0.1 mS cm^{-1} at 30 °C. The advantageous point of the electrolyte films is their preparation procedure, which needs no initiator which will produce some contaminations in the electrolyte films. The

* Corresponding author. Tel.: +81 836 85 9282; fax: +81 836 85 9201.
E-mail address: tsutsumi@yamaguchi-u.ac.jp (H. Tsutsumi).

0378-7753/$ – see front matter © 2009 Elsevier B.V. All rights reserved.
doi:10.1016/j.jpowsour.2009.11.042

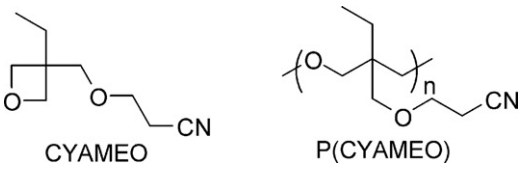

Fig. 1. Structures of CYAMEO and P(CYAMEO).

lithium salts can initiate ring-opening polymerization of the oxetane monomers [7–9].

This paper reports on a polymer with TMO units and nitrile side chains (Fig. 1) and its structure and performance as a matrix of solid polymer electrolytes. FTIR, solid state ^{7}Li NMR, and conductivity measurements provide us with detail information about lithium ions in the poly(oxetane)-based matrix.

2. Experimental

2.1. Materials

3-Ethyl-3-hydoxymethyloxetane was gifted from Ube Industries Ltd. (Japan) and used after distillation under the reduced pressure. All chemicals were purchased and used without further purification unless otherwise mentioned.

2.2. Preparation of oxetane monomer

Oxetane monomer which is possessed of nitrile group, 3-(2-cyanoethoxymethyl)-3-ethyloxetane, CYAMEO (Fig. 1), was prepared from 3-ethyl-3-hydroxymethyloxetane (EHO) and acrylonitrile under similar procedure reported by Ye et al. [11]. Typical preparation procedure is as follows: the mixture with EHO (23.22 g, 0.198 mol), acrylonitrile (21.78 g, 0.410 mol) and water (10 ml) was stirred under room temperature. Twenty percent of tetraethylammonium hydroxide solution (2.6 ml) was added to the mixture and then stirred for 19 h at room temperature. The reaction mixture was extracted with diethyl ether (100 ml) and the ether solution was washed with water (50 ml), twice. After the ether solution was dried with magnesium sulfate, the ether was removed with a rotary evaporator. The residue was distilled under reduced pressure and the fraction (160–185 °C, 133–266 Pa) was corrected. Yield: 22.7 g, 67%.

The structure of 3-(2-cyanoethoxymethyl)-3-ethyloxetane was confirmed with NMR and FTIR measurements.

^{1}H NMR (δ, ppm from TMS in $CDCl_3$): 0.90 (t, 3H, $J_{CH_3-CH_2}$ = 7.42 Hz, –C$\underline{H}_3$), 1.76 (q, 2H, $J_{CH_2-CH_3}$ = 7.42 Hz, –C$\underline{H}_2$CH$_3$), 2.44 (t, 2H, $J_{CH_2-CH_2}$ = 6.43 Hz, –C$\underline{H}_2$CH$_2$–CN), 3.63 (s, 2H, –C–C$\underline{H}_2$–O–), 3.72 (t, 2H, $J_{CH_2-CH_2}$ = 6.43 Hz, –CH$_2$C$\underline{H}_2$–CN), 4.44 (dd, 4H, $J_{-CH_2-O-CH_2-}$ = 5.94, 12.37 Hz, ring, –C$\underline{H}_2$–O–C$\underline{H}_2$–).

FTIR (cm^{-1}): 978 cm^{-1} (ring's C–O–C), 1114 cm^{-1} (C–O–C), 2251 cm^{-1} (CN), 2800–3000 cm^{-1} (CH$_2$).

2.3. Polymerization of 3-(2-cyanoethoxymethyl)-3-ethyloxetane

Ring-opening polymerization of 3-(2-cyanoethoxymethyl)-3-ethyloxetane, CYAMEO, was initiated with boron trifluoride diethyl ether complex (BF_3·Et_2O) and 1,4-butandiol [11]. A tri-necked round flask (100 ml) was filled with nitrogen and CYAMEO (5.94 g, 0.035 mol), dichloromethane (5 ml) and 1,4-butanediol (100 μl) were added to the flask and stirred at 0 °C for 30 min. Initiator, BF_3·Et_2O (100 μl) was added to the flask and stirred at −5 °C for 6 h. After the polymerization, the mixture was added to ethanol (300 ml) and the precipitated polymer was corrected with a glass filter and removed the ethanol under reduced pressure (*ca.* 266 Pa) at 40 °C for 12 h. Yield: 0.954 g, 16%

The structure of poly(3-(2-cyanoethoxymethyl)-3-ethyloxetane), P(CYAMEO), was confirmed with NMR and FTIR measurements. The number-averaged molecular weight of P(CYAMEO) was estimated with relative intensities of the NMR peaks between the terminal structure (3.32 ppm) and the main chains (3.24 ppm).

^{1}H NMR (δ, ppm from TMS in $CDCl_3$). Repeating unit: 0.86 (t, $J_{CH_3-CH_2}$ = 7.25 Hz, –C$\underline{H}_3$), 1.39 (q, $J_{CH_2-CH_3}$ = 7.25 Hz, –C$\underline{H}_2$CH$_3$), 2.60 (t, $J_{CH_2-CH_2}$ = 5.94 Hz, –C$\underline{H}_2$CH$_2$CN), 3.24 (s, –C$\underline{H}_2$–), 3.36 (s, –C$\underline{H}_2$–), 3.62 (t, $J_{-CH_2-CH_2-}$ = 5.94 Hz, –CH$_2$C$\underline{H}_2$CN). Terminal group: 0.55 (t, $J_{CH_3-CH_2}$ = 7.25 Hz, –C$\underline{H}_3$), 1.03 (q, $J_{CH_2-CH_3}$ = 7.25 Hz, –C$\underline{H}_2$CH$_3$), 2.60 (t, $J_{CH_2-CH_2}$ = 5.94 Hz, –C$\underline{H}_2$CH$_2$CN), 3.32 (s, –C$\underline{H}_2$–), 3.49 (s, –C$\underline{H}_2$–), 3.72 (t, $J_{-CH_2-CH_2-}$ = 5.94 Hz, –CH$_2$C$\underline{H}_2$CN).

FTIR (cm^{-1}): 1105 cm^{-1} (C–O–C), 2251 cm^{-1} (CN), 2800–3000 cm^{-1} (CH$_2$).

2.4. Preparation of P(CYAMEO)-based polymer electrolyte films

Solid polymer electrolyte films (P(CYAMEO)*n*(LiX)*m*) were prepared by casting the acetonitrile solution that contains P(CYAMEO) and LiX (X = ClO_4, BF_4, CF_3SO_3, or N(CF_3SO_2)$_2$) on an Al foil dish and removing the solvent. The molinity of the typical film, P(CYAMEO)10(LiN(CF_3SO_2)$_2$)1, was 0.59 mol kg^{-1}.

2.5. Measurements

An electrolyte film was sandwiched with two stainless steel plates (13 mm in diameter). The conductivity of the electrolyte film was measured with an LCR meter (HIOKI 3532-80 chemical impedance meter, 100 mV$_{p-p}$, 10–100 kHz) under various temperature conditions from 20 °C to 70 °C. Infrared spectra of samples were recorded with an FTIR spectrophotometer (IRPresatge-21, Shimadzu). ^{1}H NMR spectra of CYAMEO and P(CYAMEO) were obtained on an NMR spectrophotometer (EX-270 or GSX-270, JEOL). XRD patterns of the composites films were recorded with an X-ray diffraction meter (XD-D1, Shimadzu, CuKα, λ = 0.1542 nm). DSC measurements of the samples were preformed with a differential scanning calorimeter (DSC5100S, Bruker AXS), heating rate was 10 K min^{-1}.

Solid state ^{7}Li NMR spectra were recorded at 116.9 MHz on a Chemagnetics CMX-300 spectrometer. Approximately 10 mg of sample was inserted into a 4.0-mm rotor. Samples were spun at the magic angle at 6000 Hz. The chemical shifts were externally referred to lithium ion of 1 mol l^{-1} LiCl/D_2O solution. The spin lattice relaxation time, T_1, was determined by inversion recovery pulse sequence (180° pulse–τ–90° pulse).

Cyclic voltammetry measurements were performed with a three-electrode cell. The cell had a nickel plate (5 mm × 5mm) as a working electrode, a lithium tip (2.5 mm × 5 mm) as a reference electrode, and a lithium foil (10 mm × 10 mm) as a counter electrode. A P(CYAMEO)-based electrolyte film was sandwiched with these electrodes. The similar cell configuration was reported in our previous paper [16]. The voltammograms were recorded with a computer-controlled potentiogalvanostat (HSV-100, Hokuto denko) under Ar atmosphere (dew point was at −70 °C) at 55 °C.

3. Results and discussion

3.1. Structure of P(CYAMEO)-based electrolyte films

Ring-opening polymerization of 3-(2-cyanoethoxymethyl)-3-ethyloxetane (CYAMEO) was performed with BF_3·Et_2O and 1,4-butanediol as an initiator system [11]. The structure of P(CYAMEO), Fig. 1, was confirmed with NMR and FTIR measurements. The number-averaged molecular weight of P(CYAMEO) was

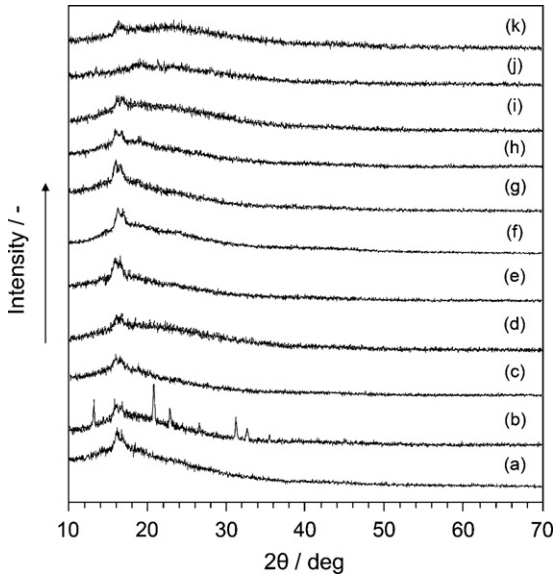

Fig. 2. X-ray diffraction patterns of P(CYAMEO) and P(CYAMEO)-based electrolyte films P(CYAMEO)n(LiX)1, (a) P(CYAMEO), (b) $n=5$, X = ClO_4, (c) $n=10$, X = ClO_4, (d) $n=20$, X = ClO_4, (e) $n=40$, X = ClO_4, (f) $n=10$, X = BF_4, (g) $n=20$, X = BF_4, (h) $n=10$, X = CF_3SO_3, (i) $n=20$, X = CF_3SO_3, (j) $n=10$, X = $N(CF_3SO_2)_2$, and (k) $n=20$, X = $N(CF_3SO_2)_2$.

6430 which is estimated from the NMR results. P(CYAMEO) has three possible sites which coordinate to lithium ions. One is a nitrile group in the side chains; others are oxygen atoms in ether moiety in the main chain and the side chain, respectively.

Fig. 2 shows the X-ray diffraction patterns of P(CYAMEO) and P(CYAMEO)-based electrolyte films with various lithium salts. The broad peaks at around 16° (Fig. 2(a)) are attributed to the amorphous structure of the P(CYAMEO) matrix. The electrolyte film with higher salt content (P(CYAMEO)5($LiClO_4$)1 film, Fig. 2(b)) shows some sharp peaks which are attributed to undissolved lithium salt. The molinity of P(CYAMEO)5($LiClO_4$)1 is about 1.18 mol kg^{-1}. The electrolyte films with lower salt content, the molar ratio of lithium salt to repeating unit of P(CYAMEO) is 1/40, 1/20, and 1/10, have no obvious sharp peaks which are attributed to lithium salts. This indicates that the P(CYAMEO) matrix is effective to dissolve lithium salt.

Fig. 3 shows the expanded FTIR spectra from 2220 cm^{-1} to 2320 cm^{-1} of P(CYAMEO) and P(CYAMEO)-based electrolyte films with various lithium salts, P(CYAMEO)10(LiX)1, X = ClO_4, BF_4, CF_3SO_3 and $N(CF_3SO_2)_2$. The peak at 2250 cm^{-1} of P(CYAMEO) matrix is attributed to the stretch vibration mode of nitrile group. The shoulder peak at 2275 cm^{-1} is observed in the P(CYAMEO)-based electrolyte films with lithium salt. The appearance of the new shoulder peak reflects the interaction between the lithium ions and the nitrile group of P(CYAMEO) molecules. Similar shoulder appearance is reported in polyacrylonitrile-based electrolyte films [17,18]. The lithium ion has an empty orbit and the nitrogen atom in the nitrile group has a pair of unbounded electrons. Therefore, the lithium ion can bond with the nitrogen atom in the nitrile group and the electron density changes after bond formation. For nitrile bond carbon and nitrogen are conjugated with a triple bond and double bond [19]. Adding a compound (lithium ions, in this case) capable of bonding with nitrile causes the conjugated bond to disappear. The carbon and nitrogen exist as a triple bond and the bonding strength increases. Thus, the peaks at higher wave numbers would appear. Variation of lithium salts (*i.e.* kind of anion) does not affect the peak intensity at 2275 cm^{-1} in Fig. 3(b)–(e). This means that the peak shift depends on the existence of lithium ions, not anion, in the P(CYAMEO) matrix.

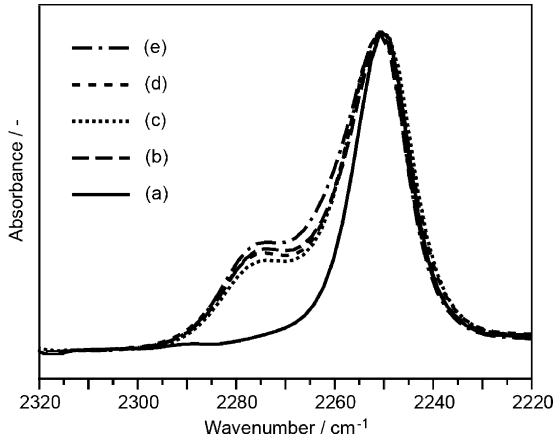

Fig. 3. Expanded FTIR spectra (from 2220 cm^{-1} to 2320 cm^{-1}) of P(CYAMEO) and P(CYAMEO)-based electrolyte films, (a) P(CYAMEO), and P(CYAMEO)10(LiX)1, (b) X = ClO_4, (c) X = BF_4, (d) X = CF_3SO_3, and (e) X = $N(CF_3SO_2)_2$.

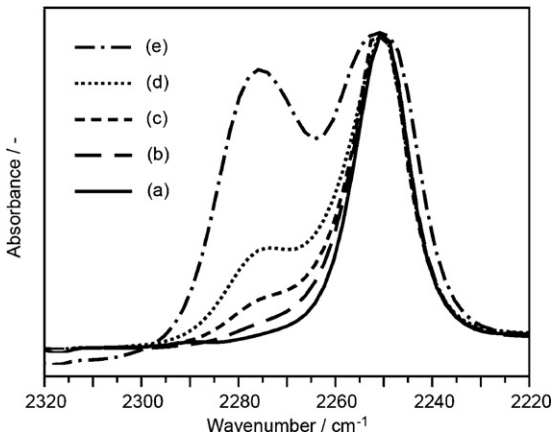

Fig. 4. Expanded FTIR spectra (from 2220 cm^{-1} to 2320 cm^{-1}) of P(CYAMEO) and P(CYAMEO)-based electrolyte films, (a) P(CYAMEO), and P(CYAMEO)n($LiClO_4$)1, (b) $n=40$, (c) $n=20$, (d) $n=10$, and (e) $n=5$.

Fig. 4 shows the expanded FTIR spectra from 2220 cm^{-1} to 2320 cm^{-1} of P(CYAMEO) and P(CYAMEO)n($LiClO_4$)1 electrolyte films ($n=5$, 10, 20 and 40). All spectra are normalized with the peak height at 2250 cm^{-1}. The peak shift is observed with the P(CYAMEO) electrolyte films with various lithium salt concentrations. The peak intensity at 2275 cm^{-1} increases with increase in salt concentration in the P(CYAMEO)-base electrolyte films. This suggests that increase in the number of lithium ions in the matrix enhances the number of the nitrile groups interacted with lithium ions. Table 1 shows the results of area ratio of peak which is attributed to the free nitrile and that is to the coordinated nitrile. In the P(CYAMEO)5($LiClO_4$)1 electrolyte film *ca.* 46% of the nitrile groups in the matrix interact with the lithium ions. The molar percentage of the lithium ions to the repeating units of P(CYAMEO) in the electrolyte film is 17%. The number of the coordinated nitrile groups to one lithium ion (N_c) is 2.7. In the P(CYAMEO)40($LiClO_4$)1 the N_c is 3.8. The coordination of one lithium ion to the some nitrile groups supplies high dissolution performance of the P(CYAMEO) matrix. The results suggest that the lithium ions in the P(CYAMEO) matrix interact with the nitrile groups, mainly.

Figs. 5 and 6 show the solid state ^7Li NMR spectra of the P(CYAMEO)10(LiX)1, X = $N(CF_3SO_2)_2$ or BF_4, at various temperatures (from −30 °C to 50 °C). The spectra of P(CYAMEO)10($LiN(CF_3SO_2)_2$) have a peak at *ca.* −1.2 ppm. Other P(CYAMEO)-based electrolyte films with lithium salts, except for $LiBF_4$, shows similar spectra. The spectra of P(CYAMEO)10($LiBF_4$)1

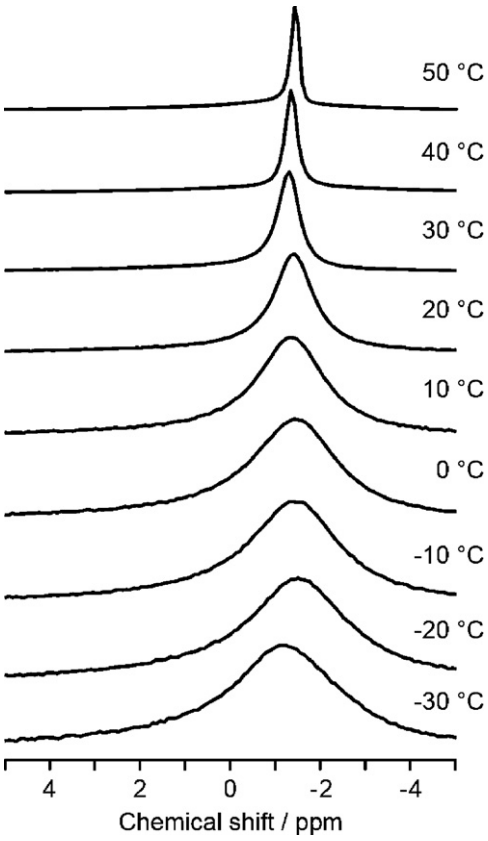

Fig. 5. Solid state ^{7}Li NMR spectra of P(CYAMEO)10(LiN(CF_3SO_2)$_2$)1 electrolyte films under various temperature conditions.

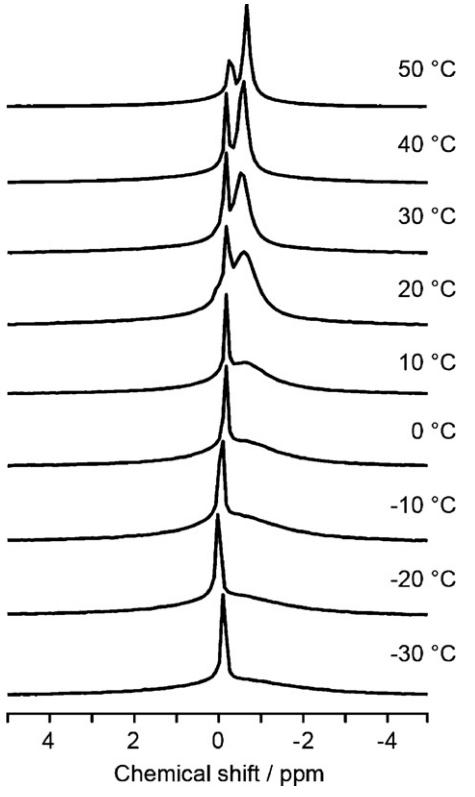

Fig. 6. Solid state ^{7}Li NMR spectra of P(CYAMEO)10($LiBF_4$)1 electrolyte films under various temperature conditions.

Table 1
Peak fitting results of nitrile peak in P(CYAMEO)-based electrolytes, P(CYAMEO)n(LiX)1.

Electrolyte		Peak area ratio (%)	
n	X	Coordinated nitrile	Free nitrile
5	ClO_4	46.4	53.6
10	ClO_4	33.2	66.8
20	ClO_4	18.1	81.9
40	ClO_4	9.2	90.8
10	BF_4	28.1	71.9
20	BF_4	17.2	82.8
10	CF_3SO_3	30.4	69.6
20	CF_3SO_3	16.8	83.2
10	$N(CF_3SO_2)_2$	35.7	64.3
20	$N(CF_3SO_2)_2$	17.2	82.8

electrolyte film have two overlapping peaks as shown in Fig. 6, especially higher temperature range (from 20 °C to 50 °C). The results suggest that the lithium ions in the matrix exist in two different chemical environments of P(CYAMEO) electrolyte with $LiBF_4$ at higher temperature (>20 °C). Detailed reason or mechanism is not clear in our investigation.

Fig. 7 shows the temperature dependence of T_1 of ^{7}Li nuclear. T_1 curves with a well-defined T_1 minimum (T_{1min}) are observed for all electrolytes. A approximately common slope on the low-temperature side of the T_1 minima and a common value of the T_{1min} were observed for all the P(CYAMEO)-based electrolyte films. The results suggest that a diffusion mechanism of the Li ions in the electrolyte is similar to each electrolyte films. Analysis of the relaxation data based on Bloembergen–Purcell–Pound (BPP) model is performed for the electrolytes [20]. The estimated K, τ_0, and E_a are listed in Table 2. K depends on the particular spin interaction responsible for the relaxation. τ_0 is the average dwell or "rattling" time for a lithium ion in a potential well before hopping to a next site. E_a is the activation energy. The K values for all electrolyte films are 1.75–2.54 × 10^9 s^{-2}. This suggests that spin interaction responsible for the relaxation is very similar to each electrolyte films. Larger τ_0 value is indicates the mobility of lithium ions is slower in the matrix. The τ_0 value of P(CYAMEO)10(LiN(CF_3SO_2)$_2$)1 electrolyte film is smaller than those of other electrolyte films. This suggests that the lithium ions in the P(CYAMEO)10(LiN(CF_3SO_2)$_2$)1

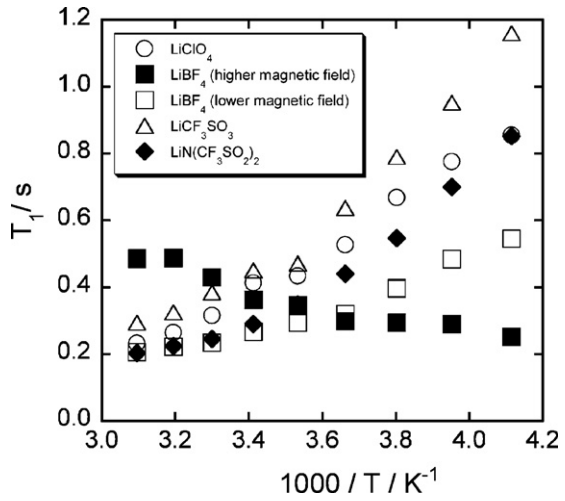

Fig. 7. ^{7}Li nuclear spin-lattice relaxation times (T_1) for P(CYAMEO)-based electrolyte films, P(CYAMEO)10(LiX)1, plotted as a function of inverse temperature, open circle: X = ClO_4, open square: X = BF_4 (higher magnetic field peak), closed square: X = BF_4(lower magnetic field), open triangle: X = CF_3SO_3, and closed diamond: X = $N(CF_3SO_2)_2$.

Table 2
T_1 fitting parameters.

Electrolyte	K (10^9 s^{-2})	τ_0 (10^{-12} s)	E_a (kJ mol^{-1})
P(CYAMEO)10($LiClO_4$)1	2.22	3.54	15.6
P(CYAMEO)10($LiBF_4$)1[a]	2.05[b] 2.50[c]	4.97[b] 7.17[c]	10.0[b] 13.4[c]
P(CYAMEO)10($LiCF_3SO_3$)1	1.75	2.43	16.5
P(CYAMEO)10($LiN(CF_3SO_2)_2$)1	2.54	1.60	17.5

[a] ^{7}Li NMR spectra of the electrolyte have two peaks.
[b] Higher magnetic field peak.
[c] Lower magnetic field peak.

electrolyte have higher mobility than in other P(CYAMEO)-based electrolytes.

3.2. Conductivity of P(CYAMEO)-based electrolyte films with various lithium salts

As mentioned in previous section, the P(CYAMEO) matrix can dissolve various lithium salts in it. The temperature dependence of conductivity for P(CYAMEO)-based electrolyte films with various lithium salts is shown in Fig. 8. The conductivity for P(CYAMEO)10(LiX)1 electrolyte film at 30 °C is 19.6 μS cm^{-1} (X = ClO_4), 6.59 μS cm^{-1} (BF_4), 6.54 μS cm^{-1} (CF_3SO_3), and 25.0 μS cm^{-1} ($N(CF_3SO_2)_2$). The conductivity for the electrolyte with $LiClO_4$ and $LiN(CF_3SO_2)_2$ is about 3–4 times higher than that with other lithium salts. The conductivity for all P(CYAMEO)-based electrolyte films increase with elevation of temperature. The conductivity at 70 °C is 0.74 mS cm^{-1} (X = ClO_4), 0.28 mS cm^{-1} (BF_4), 0.29 mS cm^{-1} (CF_3SO_3), and 0.73 mS cm^{-1} ($N(CF_3SO_2)_2$). The conductivity is 30 times enhanced by elevation of temperature. Glass transition temperature (T_g) of P(CYAMEO) and P(CYAMEO)-based electrolyte films are listed in Table 3. The T_g of P(CYAMEO) is −13.5 °C. The T_g of P(CYAMEO)10(LiX) is −18.6 °C (X = ClO_4), −17.9 °C (BF_4), −18.2 °C (CF_3SO_3), and −20.6 °C ($N(CF_3SO_2)_2$). Addition of lithium salt to P(CAYMEO) matrix do not increase in T_g value of P(CYAMEO). T_g of polyethylene oxide (PEO)-based electrolytes is normally increases with increasing inorganic salt content [21]. The cation-oxygen binding energy, which is the driving force for salt dissolution, contributes to the increase in the barrier to rotation of the polymer segments. The lithium ions in the P(CYAMEO) matrix do not have strong interaction with the oxygen atoms on the main chain of the matrix because of steric hindrance of the ethyl groups on the main chain. Thus, increase in T_g of the P(CYAMEO)-based electrolytes is not observed.

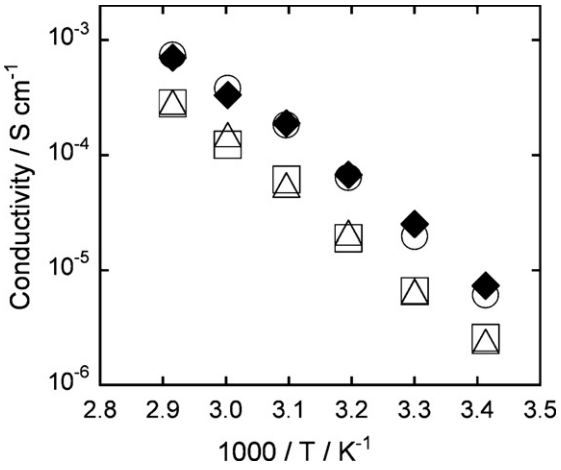

Fig. 8. Temperature dependence of conductivity for P(CYAMEO)-based electrolyte films with various lithium salts, P(CYAMEO)10(LiX)1, open circle: X = ClO_4, open square: X = BF_4, open triangle: X = CF_3SO_3, and closed diamond: X = $N(CF_3SO_2)_2$.

Table 3
Glass transition temperature of P(CYAMEO)-based electrolyte films, P(CYAMEO)n(LiX)1.

Electrolyte		T_g (°C)[a]
n	X	
5	ClO_4	−18.7
10	ClO_4	−18.6
20	ClO_4	−16.0
40	ClO_4	−12.3
10	BF_4	−17.9
20	BF_4	−16.1
10	CF_3SO_3	−18.2
20	CF_3SO_3	−18.5
10	$N(CF_3SO_2)_2$	−20.6
20	$N(CF_3SO_2)_2$	−13.5

[a] T_g of P(CYAMEO) is −13.5 °C.

VTF fitting was applied to P(CYAMEO)-based electrolyte films with various lithium salts. The VTF expression is represented by

$$\sigma = AT^{-1/2}\exp\left[\frac{-B}{R(T-T_0)}\right] \quad (1)$$

where A is the pre-exponential factor, which is related to the number of charge carriers, B is the pseudo-activation energy of ion transport, R is the gas constant, 8.314 J K^{-1} mol^{-1}, and T_0 is defined as the temperature at which the configurational entropy becomes zero, *i.e.*, the disappearance of the free volume is complete. The values of T_0 are 50 K below the glass transition temperature, according to Adam–Gibbs analysis [22]. Fig. 9 shows the VTF plots of the P(CYAMEO)-based electrolyte films and the parameters of VTF equation are summarized in Table 4. The A for P(CYAMEO)5($LiClO_4$)1 electrolyte film is very large. This indicates that the number of charge carrier in the electrolyte film is larger than other electrolyte films. The B for the P(CYAMEO)-based electrolyte films is in the range from 8.19 kJ mol^{-1} to 14.92 kJ mol^{-1}. The activation energy values estimated from the VTF equation are almost comparable with the results from the NMR analysis (Table 2).

Fig. 10 shows the relationships between salt molar fraction and conductivity for P(CYAMEO)n($LiClO_4$)1 electrolyte films. The conductivity for the P(CYAMEO)-based electrolyte films increases with increase in salt molar fraction (from 0.024 to 0.091). Further addition of $LiClO_4$ to the polymer matrix decreases in conductivity for the electrolyte film (P(CYAMEO)5($LiClO_4$)1). X-ray diffraction

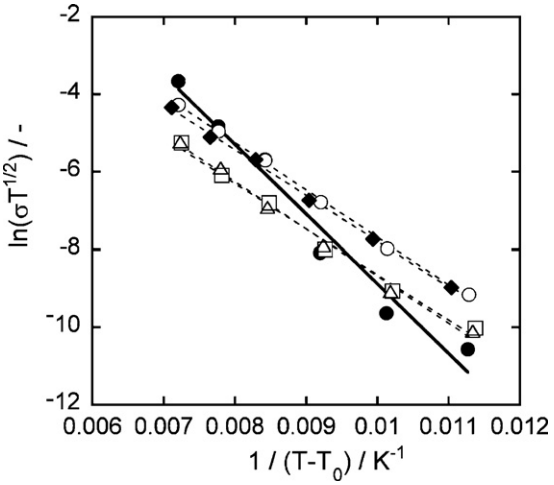

Fig. 9. Typical VTF fitting curves for P(CYAMEO)-based electrolyte, P(CYAMEO)n(LiX)1, closed circle: n = 5, X = ClO_4, open circle: n = 10, X = ClO_4, open square: n = 10, X = BF_4, open triangle: n = 10, X = CF_3SO_3, and closed diamond: n = 10, X = $N(CF_3SO_2)_2$.

Table 4
VTF parameters for the P(CYAMEO)-based electrolytes with various lithium salts, P(CYAMEO)*n*(LiX)1.

Electrolyte		VTF parameters	
n	X	A (S cm^{-1} $K^{1/2}$)	B (kJ mol^{-1})
5	ClO_4	8704.5	14.92
10	ClO_4	90.7	10.14
20	ClO_4	32.4	9.87
40	ClO_4	3.7	8.82
10	BF_4	22.4	9.77
20	BF_4	8.8	9.29
10	CF_3SO_3	31.7	10.09
20	CF_3SO_3	1.6	8.19
10	$N(CF_3SO_2)_2$	54.4	9.80

pattern for the electrolyte film suggests that some amount of undissolved lithium salt exists in it. The salt crystals prevent ions and polymers moving in the electrolyte film.

3.3. Electrochemical deposition and dissolution of lithium in P(CYAMEO)-based electrolytes

Electrochemical deposition and dissolution of lithium in an electrolyte system is a key reaction for application of the electrolyte to lithium metal secondary batteries. We demonstrated electrochemical deposition and dissolution of lithium in the P(CYAMEO)-based electrolytes. Fig. 11 shows the cyclic voltammograms of a nickel

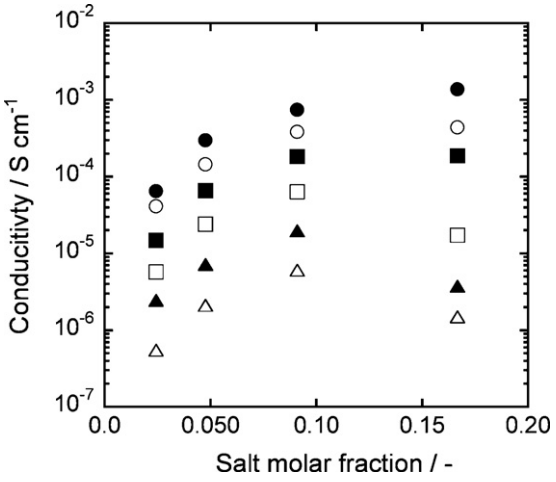

Fig. 10. Plots as a function of the salt molar fraction of the conductivity for P(CYAMEO)-based electrolyte films, P(CYAMEO)*n*($LiClO_4$)1, measured at various temperatures—open triangle: 20 °C, closed triangle: 30 °C, open square: 40 °C, closed square: 50 °C, open circle: 60 °C, and closed circle: 70 °C.

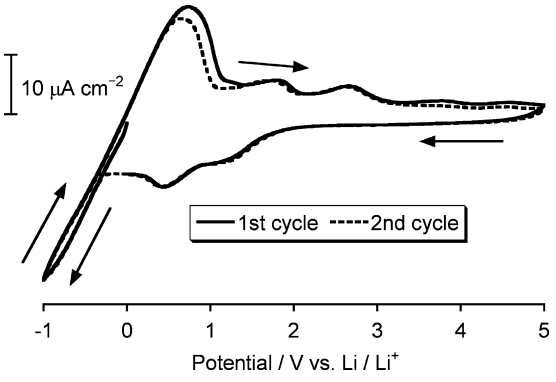

Fig. 11. Cyclic voltammograms for a nickel plate in the P(CYAMEO)10(LiN(CF_3SO_2)$_2$)1 electrolyte film at 55 °C, scan rate 1 mV s^{-1}.

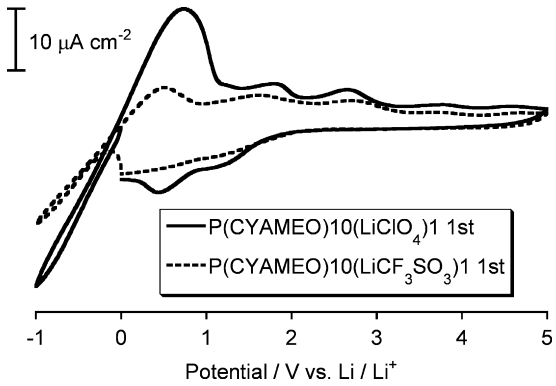

Fig. 12. Cyclic voltammograms for a nickel plate in the P(CYAMEO)10(LiX)1 electrolyte film at 55 °C, scan rate 1 mV s^{-1}, solid line: X = $N(CF_3SO_2)_2$, dotted line: ClO_4.

(Ni) electrode in the P(CYAMEO)10(LiN(CF_3SO_2)$_2$)1 electrolyte film. In anodic scan (from 0 V to −1 V vs. Li/Li$^+$) increase in current is attributed to the lithium deposition process on the Ni electrode. Cathodic peak at 0.688 V vs. Li/Li$^+$ which is due to dissolution of lithium from the Ni plate is also observed. Similar electrochemical response is observed in second potential scan.

Fig. 12 shows the cyclic voltammograms of a Ni electrode in P(CYAMEO)10(LiX)1, X = ClO_4 or $N(CF_3SO_2)_2$, electrolyte film. Similar electrochemical responses are observed in the electrochemical cell with the electrolyte films. However, the current density in the P(CYAMEO)-based electrolyte with LiN(CF_3SO_2)$_2$ is lower than that with $LiClO_4$. This suggests that the P(CYAMEO)-based electrolyte with LiN(CF_3SO_2)$_2$ is more suitable for application to secondary batteries.

4. Conclusions

We prepared the solvent-free polymer electrolyte films with trimethylene oxide which are synthesized by ring-opening polymerization of the oxetane with nitrile group, CYAMEO. The P(CYAMEO) matrix can dissolve various lithium salts, such as $LiClO_4$, LiN(CF_3SO_2)$_2$.

The conductivity at 30 °C for P(CYAMEO)-based electrolyte films, P(CYAME)10(LiX)1, is 19.6 μS cm^{-1} (X = $LiClO_4$), 6.59 μS cm^{-1} (BF_4), 6.54 μS cm^{-1} (CF_3SO_3), and 25.0 μS cm^{-1} ($N(CF_3SO_2)_2$). The rise in temperature from 30 °C to 70 °C increases their conductivity, about 30–40 times. The conductivity at 70 °C for P(CYAMEO)-based electrolyte films is 0.742 mS cm^{-1} (X = $LiClO_4$) and 0.703 mS cm^{-1} ($N(CF_3SO_2)_2$). Spectroscopic results suggests that the lithium ions in the P(CYAMEO) matrix strongly interacted with the nitrile groups not oxygen atoms in the matrix. Solid state ^{7}Li NMR results suggest that the mobility of lithium ions in the P(CYAMEO) matrix is affected with the kind of lithium salts.

The plating and dissolution of lithium on the nickel electrode in the P(CYAMEO) electrolyte film with LiN(CF_3SO_2)$_2$ are clearly observed by cyclic voltammetry measurements. The P(CYAMEO) electrolyte film with LiN(CF_3SO_2)$_2$ is the suitable system, which we prepared in this investigation, because of higher conductivity and better electrochemical response of lithium deposition and dissolution on a Ni plate.

Acknowledgements

This work was financially supported by a program of "Development of High-performance Battery System for Next-generation Vehicles, Li-EAD" from the New Energy and Industrial Technology Development Organization (NEDO) of Japan and the Electric Technology Research Foundation of Chugoku.

References

[1] B. Scrosati, C.A. Vincent, MRS Bulletin 25 (2000) 28–30.
[2] A. Manuel Stephan, European Polymer Journal 42 (2006) 21–42.
[3] O. Buriez, Y.B. Han, J. Hou, J.B. Kerr, J. Qiao, S.E. Sloop, M. Tian, S. Wang, Journal of Power Sources 89 (2000) 149–155.
[4] Y. Ma, M. Doyle, T.F. Fuller, M.M. Doeff, L.C. De Jonghe, J. Newman, Journal of the Electrochemical Society 142 (1995) 1859–1868.
[5] Z.G. Feng, Y.M. Zhao, L. Ye, Y. Bai, F. Wu, Beijing Ligong Daxue Xuebao/Transaction of Beijing Institute of Technology 26 (2006) 1098–1103.
[6] Y.E. Lin, F. Zeng-Guo, Z. Yu-Mei, W. Feng, C. Shi, W. Guo-Qing, Journal of Polymer Science, Part A: Polymer Chemistry 44 (2006) 3650–3665.
[7] Y. Miwa, H. Tsutsumi, T. Oishi, Polymer Journal 33 (2001) 927–933.
[8] Y. Miwa, H. Tsutsumi, T. Oishi, Polymer Journal 33 (2001) 568–574.
[9] Y. Miwa, H. Tsutsumi, T. Oishi, Electrochemistry 70 (2002) 264–269.
[10] L. Ye, Z.G. Feng, S.T. Li, F. Wu, S. Chen, G.Q. Wang, Gaodeng Xuexiao Huaxue Xuebao/Chemical Journal of Chinese Universities 26 (2005) 1946–1951.
[11] L. Ye, Z.G. Feng, Y.F. Su, F. Wu, S. Chen, G.Q. Wang, Polymer International 54 (2005) 1440–1448.
[12] L. Ye, Z.G. Feng, X.W. Zhang, Q. Qin, Y. Bai, F. Wu, S. Chen, G.Q. Wang, Chinese Journal of Polymer Science 24 (2006) 503–513 (English Edition).
[13] L. Ye, P. Gao, F. Wu, Y. Bai, Z.G. Feng, Polymer 48 (2007) 1550–1556.
[14] J.B. Kerr, G. Liu, L.A. Curtiss, P.C. Redfern, Electrochimica Acta 48 (2003) 2305–2309.
[15] G. Liu, C.L. Reeder, X. Sun, J.B. Kerr, Solid State Ionics 175 (2004) 781–783.
[16] H. Tsutsumi, M. Yamamoto, M. Morita, Y. Matsuda, T. Nakamura, H. Asai, Journal of Power Sources 41 (1993) 291–298.
[17] B. Huang, Z. Wang, L. Chen, R. Xue, F. Wang, Solid State Ionics 91 (1996) 279–284.
[18] Z. Wang, B. Huang, H. Huang, L. Chen, R. Xue, F. Wang, Electrochimica Acta 41 (1996) 1443–1446.
[19] W. Gerrard, M.F. Lappert, H. Pyszora, J.W. Wallis, Journal of the Chemical Society (Resumed) (1960) 2182–2186.
[20] S.H. Chung, K.R. Jeffrey, J.R. Stevens, The Journal of Chemical Physics 94 (1991) 1803–1811.
[21] A. Vall, S. Besner, J. Prud'Homme, Electrochimica Acta 37 (1992) 1579–1583.
[22] G. Adam, J.H. Gibbs, The Journal of Chemical Physics 43 (1965) 139–146.